Search for strongly blue axion isocurvature

Daniel J. H. Chung* and Amol Upadhye†
Department of Physics, University of Wisconsin-Madison, Madison, Wisconsin 53706, USA

(Received 19 December 2017; published 18 July 2018)

It is known that if the Peccei-Quinn symmetry-breaking field is displaced from its minimum during inflation, the axion isocurvature spectrum is generically strongly blue tilted with a break transition to a flat spectrum. We fit this spectrum (incorporated into the "vanilla" Λ-CDM cosmological model) to the Planck and BOSS DR11 data to assess how much the existing data can accommodate the presence of axionic blue-tilted isocurvature perturbations. We find that the preferred parameter region is consistent with all of the dark matter being composed of QCD axions in the context of inflationary cosmology with an expansion rate of order 10^8 GeV, the axion decay constant of order 10^{13} GeV, and the initial misalignment angle of order unity. The data are consistent with there being no isocurvature perturbations at the level of just above one sigma. Intriguingly, isocurvature with a spectral break may at least partially explain the low-ℓ vs high-ℓ anomalies seen in the CMB data.

DOI: 10.1103/PhysRevD.98.023525

I. INTRODUCTION

QCD axions [1–8] are well motivated because they represent a simple elegant solution to the strong CP problem and can be embedded in UV completions such as string theory [9]. A huge body of literature exists regarding the cosmological implications of the axions in which the field responsible for Peccei-Quinn (PQ) symmetry breaking has not been displaced from its minimum (see e.g., [10–16]). In such cases, the isocurvature spectral index n_I is very close to 1 which is often referred to as scale invariant. However, if the PQ symmetry-breaking field is displaced from its minimum during inflation, blue spectral tilted isocurvature perturbations are naturally generated [17]. Indeed, the Goldstone theorem does not apply in such cases because the axions do not represent perturbations away from the vacuum [18]. The dyanamical mechanism of the η problem [19–22], in which small corrections to the curvature of the inflaton potential violate the slow-roll conditions and hence the scale-invariance of the power spectrum, is a beneficial feature in the case of a rolling spectator field. It makes the isocurvature spectral index $n_I - 1 \sim O(1)$ generic in this class of models. Furthermore, because the radial field eventually reaches its minimum, this class of models generically predicts a break in the spectrum where the spectral index transitions to that of scale invariance. Indeed, since $n_I > 2.4$ cannot be generated with a spectator scalar field degree of freedom (d.o.f.) with a time-independent mass [23], a large spectral index in the context of inflationary cosmology predicts a break in the spectrum for strongly blue-tilted isocurvature perturbations, independently of the axion paradigm. This means interesting robust information about the physics beyond the standard model of particle physics (i.e., the existence of a time dependent mass of a new particle) can be gained from finding observational evidence for a strongly blue tilted spectrum with a break. Because the axions are arguably the best motivated underlying model for this class of scenarios producing a break spectrum, we will call this strongly blue tilted isocurvature spectrum with a break an axionic blue isocurvature (ABI) spectrum.

The break region in the ABI spectrum cannot be computed analytically using the standard techniques [18]. Recently, an efficient 3-parameter fit function $\Delta_S^2(k, k_\star, n_I, \mathcal{Q}_1)$ was constructed from generalizing a numerical investigation [24] of the model of [17], and this fit function has a bump feature that can be numerically significant at an $O(1)$ level. In this paper, we use this fit function in the context of Λ-CDM cosmological model to fit 9 parameters to the PLANCK [25,26] and Baryon Oscillation Spectroscopic Survey Data Release 11 (BOSS DR11) [27,28]. We find that the data prefer a nonzero ABI spectrum at the 1-sigma level with expectation values of about $\{k_\star/a_0 = 4.1^{+14}_{-2.7} \times 10^{-2}\ \mathrm{Mpc}^{-1}, n_I = 2.76^{+1.1}_{-0.59}, \mathcal{Q}_n = 0.96^{+0.32}_{-0.93}\}$ where $k_\star/a_0$ is the spectral location of the break, n_I is the isocurvature spectral index, and $\mathcal{Q}_n \times 10^{-10}$ is approximately the isocurvature power on BAO scales that can be compared to $\Delta_\zeta^2 \sim O(10^{-9})$ of the usual adiabatic perturbations. This preferred parameter region can be consistent with an initial axion angle of $\theta_+(t_i) = 0.1$ and all of the dark matter being made up of axions. For example, with this fiducial parameter

*danielchung@wisc.edu
†aupadhye@wisc.edu

choice, the scale of inflation is given by the expansion rate during inflation of $H \approx 2 \times 10^8$ GeV and the axion decay constant of $F_a \sim 10^{13}$ GeV. In this parameter range, the bump that was computed numerically in [24] contributes at the level of about 10% for the values of the fit parameters and changes the shape of the fit contours only slightly. We also carried out a fit with $n_I = 3.9$ and $k_\star/a_0 = 0.5/\mathrm{Mpc}$ and find a 2σ preference for a highly blue-tilted isocurvature with a power-law spectrum on observable scales.

Since the smallest length scales probed by current CMB and galaxy surveys are similar, we find the CMB data to be more constraining due to their higher precision, though of course the two sets of observables have different parametric degeneracies. There are no substantial tensions between the two data sets; the most significant changes in the vanilla parameters due to the BOSS data are the decreases in σ_8 and τ along their mutual degeneracy direction preserving $\sigma_8 e^{-\tau}$. In the isocurvature sector, we find that BOSS data increase the preference for blue-tilted models with spectral breaks below observable length scales.

The order of presentation will be as follows. In the next section, we review the fitting function $\Delta_S^2(k, k_\star, n_I, \mathcal{Q}_1)$ and a model that inspired this. In Sec. III, we present the ABI + Λ-CDM fit. In Sec. IV, we interpret the fit results in terms of the model of [17]. We conclude with a summary of the work and speculations about this work's connection to the low-ℓ and high-ℓCMB data mismatch noted in [29].

II. A BRIEF REVIEW OF THE ABI SPECTRUM PARAMETRIZATION

Most of the axionic isocurvature literature focuses on the scenario in which the Peccei-Quinn symmetry-breaking field f_{PQ} has already relaxed to the minimum of the effective potential [10–13,15,16]. However, in situations in which the radial direction has a mass of order H, such an assumption is not well justified since the inflaton itself is out of equilibrium during that time, and it may take many e-folds for f_{PQ} to relax to the minimum of the effective potential [17]. In such cases, a strongly blue-tilted isocurvature spectrum is generically generated. Particularly in supersymmetric extensions of the standard model, flat directions abound, and f_{PQ} realized as a flat direction field will generically have masses of $O(H)$ [17,18] generating dynamics suitable for the creation of ABI perturbations.[1]

Although the ABI spectrum computed in [17] is qualitatively valid, it was noted in [18] that there is generically a spectral gap in analytic computability (with the standard techniques) surrounding the break region. In [24], we computed numerically the ABI spectrum of the model analytically analyzed in [17,18] and found that the spectrum indeed has a nontrivial bump in the break region between the constant blue tilt region and the scale invariant region with the transition spectral width consistent with the predictions of [18]. The ABI spectrum including the bump is fit well with the following function defined by three parameters $k_\star$, n_I, and $\mathcal{Q}_1$:

$$\Delta_S^2(k, k_\star, n_I, \mathcal{Q}_1) \approx \mathcal{Q}_1 \frac{1 + \alpha(n_I) L\left[\frac{1}{\sigma(n_I)} \ln\left(e^{-\mu(n_I)} \frac{k}{k_\star}\right)\right] S\left[\frac{\lambda(n_I)}{\sigma(n_I)} \ln\left(e^{-\mu(n_I)} \frac{k}{k_\star}\right)\right]}{\left[1 + \left(\tilde{\rho}(n_I) 2^{2\sqrt{\frac{9}{4} - c_+(n_I)}} \frac{\Gamma^2\left(\sqrt{\frac{9}{4} - c_+(n_I)}\right)}{2\pi}\left(1 + \frac{c_+(n_I)}{0.9}\right)\left(\frac{k}{k_\star}\right)^{n_I - 1}\right)^{-1/w}\right]^w} \tag{1}$$

$$L(x) = 1/(1 + x^2) \tag{2}$$

$$S(x) = 1 + \tanh(x) \tag{3}$$

$$c_+(n_I) = \frac{1}{4}(n_I - 1)(7 - n_I). \tag{4}$$

The parameters $\{\alpha, \sigma, \mu, \lambda, w, \tilde{\rho}\}$ are numerical factors that can be deduced from an interpolation of a table of numbers given in Table 1 of [24]. Here, Δ_S^2 is the usual isocurvature power spectrum defined in Eq. (11) of [18] and Eq. (31) of [24]. The fitting function itself is accurate to 20%, with this error concentrated in the bump region. Since our best-fitting models have isocurvature power less than about 10% of adiabatic power, this amounts to about less than 2% error in the total power spectrum. We tested the sensitivity of our constraints to these errors by removing the bump entirely, through the NB models, and found very similar parameter values.

The broad features of the isocurvature power spectrum are described by the large-scale spectral index n_I, the break position $k_\star$, and the break width w. On top of this monotonic power spectrum is a peak of height α, width σ, position μ, and skewness λ, resulting from the axionic field sloshing around the minimum of its potential during the spectral transition. For example, for $n_I = 3$, the parameter set is $\{\alpha = 0.56, \sigma = 0.46, \mu = 0.126, \lambda = -0.035, w = 0.84, \tilde{\rho} = 1.2\}$. The number 0.9 in Eq. (1) corresponds to making a choice for a model dependent parameter that gives an approximate fit to model-dependent numerically computed results when this number is in the range [0.5, 1].

To test if the ABI spectrum shows up in the current data and to see how it is constrained, we fit in Sec. III the standard six "vanilla" cosmological parameters (Λ-CDM) plus up to three more parameters describing the ABI power spectrum. The

[1] Indeed, this is a situation in which the η-problem of inflation turns into an advantage.

standard vanilla Λ-CDM parameters can be given as follows: (1) n_s, the spectral index of adiabatic scalar perturbations; (2) σ_8, the root-mean-squared power in 8 Mpc$/h$ spheres where (3) $h = H_0/(100\ \mathrm{km/sec/Mpc})$, the Hubble parameter; (4) $\omega_c = \Omega_{c,0}h^2$, where $\Omega_{c,0}$ is the density fraction of cold dark matter (CDM) at the present time; (5) $\omega_b = \Omega_{b,0}h^2$, where $\Omega_{b,0}$ is the baryon density fraction; and (6) τ, the optical depth to the cosmic microwave background. Since neglecting the neutrino mass can lead to parameter biases, we fix $\omega_\nu = \Omega_\nu h^2 = 0.0006$ for the fits unless specified otherwise. For efficient Markov chain Monte Carlo (MCMC) sampling with a flat prior (i.e., to minimize degeneracies), it is useful to sample

$$Q_n \equiv 10^{10}\frac{\mathcal{Q}_1}{1+\left(\frac{k_\star}{k_0}\right)^{n_I}} \tag{5}$$

and

$$\kappa_\star = \ln\frac{k_\star}{k_0}, \tag{6}$$

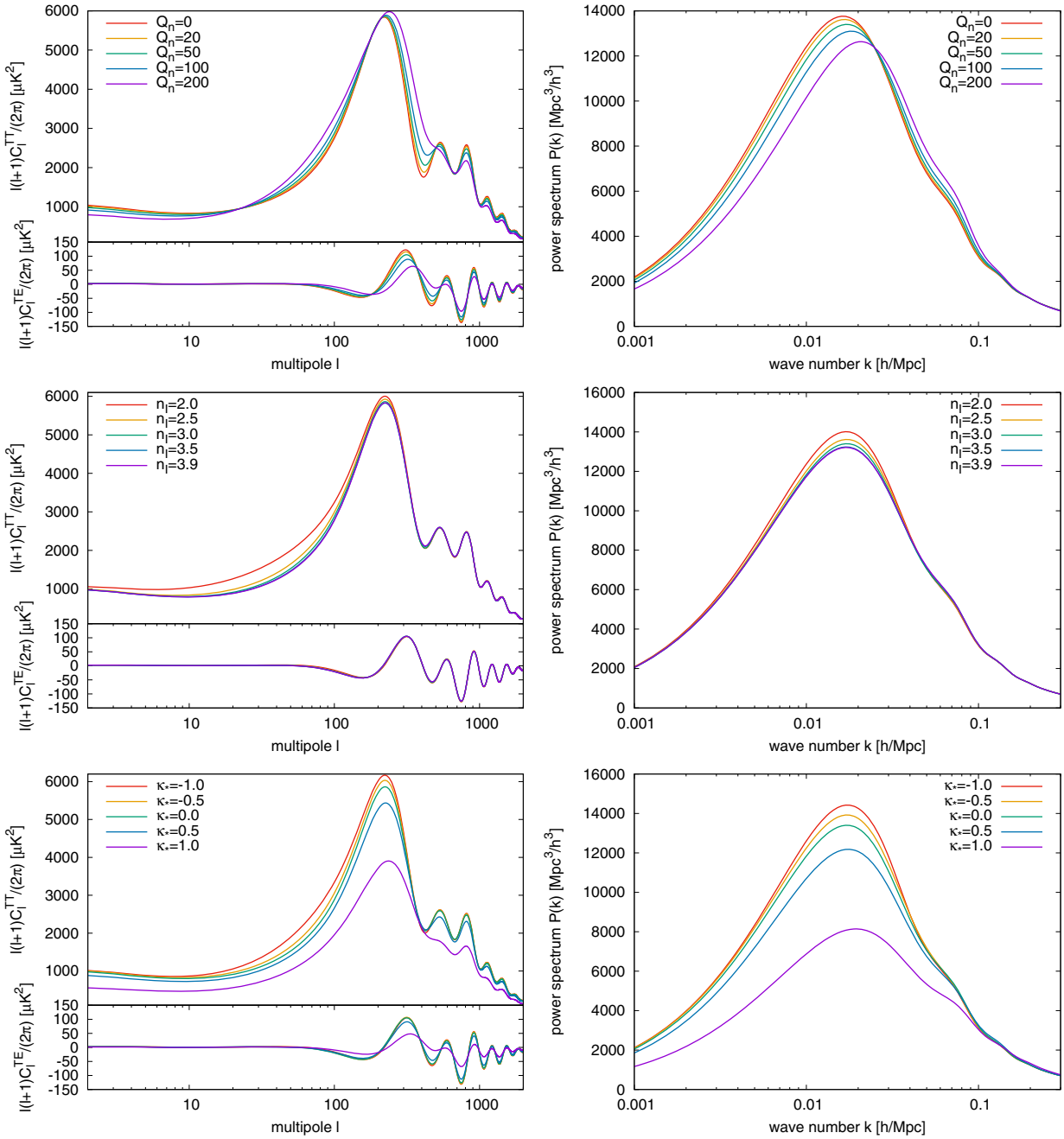

FIG. 1. Variation of the ABI parameters about the central values of $Q_n = 50$, $n_I = 3$, and $\kappa_\star = 0$. Note that Q_n has been set to a very large value in order to exaggerate the effects. (left) CMB TT and TE power spectra. (right) Matter power spectra.

(where k_0 is a fiducial wave vector which we will set as $k_0/a_0 = 0.05\ \mathrm{Mpc}^{-1}$) instead of the parameters $\mathcal{Q}_1$ and $k_\star$. Figure 1 illustrates the effects of varying Q_n, n_I, and $\kappa_\star$, using a large value of Q_n in order to make the isocurvature contribution more apparent.

III. DATA FIT

In this section, we fit the mixed adiabatic-isocurvature cosmological model presented in Sec. II to Planck and BOSS data. We broadly classify three different ABI parameter regions as follows:

(i) KK: the model of Kasuya and Kawasaki, Ref. [17], with the bump fit by Ref. [24];
(ii) NB: a no-bump version of KK, with the bump height α set to zero and the break width parameter fixed to $w = 1/3$;
(iii) PWR: a simple power-law spectrum, which we implement by fixing $\kappa_\star = \ln(200)$ in the NB model.

We are especially interested in models with the bluest tilts $n_I \lesssim 4$ over much of the observable parameter space $k \sim k_0$. Hence we also consider the following lamppost models partially restricting the allowed values of n_I and $\kappa_\star$:

(i) BLUE: the KK model with $n_I = 3.9$;
(ii) HI-BLUE: the BLUE model with the further restriction $\kappa_\star = \ln(10)$.
(iii) LAMP-N: the KK model with $\kappa_\star = \ln(N)$;

At small N, LAMP-N approaches an ordinary flat isocurvature model, while at large N it approaches a power law. We will constrain LAMP-1, LAMP-2, and LAMP-10.

A. Analysis procedure

The data analysis used here is that of Ref. [30], modified to include isocurvature perturbations. Briefly, we combine the publicly-available Planck likelihood code of Refs. [25,26] with the BOSS DR11 redshift-space galaxy power spectrum of Refs. [27,28], and explore the likelihood using a Metropolis-Hastings Markov Chain Monte Carlo algorithm with a set of flat priors given in Table I. We now summarize this analysis procedure below.

Our flat priors are chosen to be broad to allow adjustments to the vanilla parameters in response to the addition of isocurvature parameters. In particular, the priors on h, ω_b, and τ in Table I are the largest ranges allowed by the `CAMB` code of Ref. [31]. Requiring that the KK spectator fields have slow-roll solutions in the early universe restricts the range of isocurvature indices to $1 \le n_I < 4$. Our slightly narrower priors reflect the range of the fitting function of Ref. [24]. Poorly-constrained isocurvature parameters could be sensitive to our choice of flat priors through the effect pointed out in [32]. Since we do not claim significance in the fit results, we will not investigate here the fit's dependence on the different choices of priors.

Meanwhile, the prior on $\kappa_\star$ is based not on fundamental physical arguments, but on the range of scales probed by current surveys. In the limit of large positive $\kappa_\star$, the isocurvature spectrum reduces to a simple power law, and the data are insensitive to $\kappa_\star$. For very negative $\kappa_\star$, the spectral break is pushed to scales with large sample variance, and the data become insensitive to n_I as well as to $\kappa_\star$. Thus we set the minimum $k_\star$ to be a few times the horizon scale $a_0 H_0 = 3.3 \times 10^{-4} h/\mathrm{Mpc}$, and the maximum $k_\star$ to be a few times the largest wave numbers probed by Planck and BOSS. Since more advanced surveys will be able to measure larger $\kappa_\star$, we use the LAMP-10 and HI-BLUE test models to look for hints of a $\kappa_\star$ just beyond the currently-observable range.

The Planck likelihood computation is divided into low-ℓ and high-ℓ components. Since the low-ℓ polarization likelihood is computationally expensive, we restrict our $\ell < 30$ analysis to the temperature power spectrum. For $\ell \ge 30$ we employ the simplified `plik-lite` function of Ref. [26], which we marginalize over the absolute calibration parameter A_Planck as recommended. CMB power spectra are computed using the `CAMB` cosmology code of Ref. [31] modified to include isocurvature power spectra described by the fitting function of Ref. [24] appropriate to models with blue-to-flat spectral breaks. For mixed models combining adiabatic and isocurvature perturbations, we ran `CAMB` separately for adiabatic and isocurvature initial conditions, then added to find the combined linear power spectra. Since CMB lensing is a nonlinear process, we also compiled a stand-alone version of the `CAMB` CMB lensing function, which we used to lens the combined linear power spectra.

The BOSS DR11 analysis of Ref. [27] measures the monopole and quadrupole of the redshift-space galaxy power spectrum at an effective redshift of $z = 0.57$ over a range of wave numbers $0.01h/\mathrm{Mpc} \le k \le 0.2h/\mathrm{Mpc}$. That reference provides the window functions and covariance matrices necessary for comparing power spectra to the BOSS data. Beginning with `CAMB` inputs, we compute the power spectra for mixed adiabatic and isocurvature models using a modified version of the `redTime` nonlinear

TABLE I. The prior probability distribution is uniform in the parameters n_s, n_I, $\ln(\sigma_8)$, Q_n, θ_{100}, ω_c, ω_b, τ, and $\kappa_\star$, with the above bounds. θ_{100}, an approximation to the angular scale of acoustic oscillations which is related to the parameter h, is described in Sec. III of Ref. [30].

n_s	n_I	σ_8	Q_n	h	ω_c	ω_b	τ	$\kappa_\star$
>0	[1, 3.94]	>0	>0	[0.2, 1]	>0	>0.001	>0.01	$[\ln\frac{0.001/\mathrm{Mpc}}{k_0}, \ln\frac{0.5/\mathrm{Mpc}}{k_0}]$

redshift-space perturbation code of Refs. [30,33], based upon the Time-Renormalization Group method of Ref. [34]. Since the growth of large-scale structure after decoupling is well described by a single CDM + baryon fluid, mixed initial conditions can easily be accommodated by adding the linear adiabatic and isocurvature power spectra computed by CAMB at the redshift $z_{\rm in}$ at which the nonlinear perturbative computation is initialized. We choose $z_{\rm in} = 200$, as tested against N-body dark matter simulations in [33,35].

Galaxies are biased tracers of the underlying density field. Since blue-tilted isocurvature changes the shape of the matter power spectrum, we must accurately model the scale-dependence of galaxy bias. Reference [36] describes a five-parameter model of galaxy bias, which is simplified to a three-parameter model in Ref. [37]. We use this three-parameter model unless otherwise noted. At each chain point, we marginalize numerically over these bias parameters as in Ref. [30] in order to compute the likelihood.

For each model and data combination, we run 5 chains, with a total of at least 500 000 MCMC points for each Planck + BOSS analysis and 1 000 000 for each Planck-only analysis. Given the large number of points in a chain to produce independent samples and sufficient computing resources, we forgo the chain-thinning procedure. MCMC convergence is tested using the potential scale reduction factor $\sqrt{R}$, which approaches unity from above as the variance of the means of several chains becomes much smaller than the mean of the individual chain variances [38,39]. We judge each set of 5 chains to have converged when $\sqrt{R} < 1.05$ for fixed ω_ν and $\sqrt{R} < 1.1$ for variable ω_ν; these are more stringent than the convergence requirement $\sqrt{R} < 1.2$ recommended in Ref. [39].

B. CMB constraints

Marginalized constraints on the vanilla and isocurvature parameters from Planck data alone are shown in Table II. Since Refs. [40,41] caution that low-level $T \to E$ leakage may contaminate the polarization data in a way which mimics isocurvature, we begin by evaluating the effects of such leakage on our parameter constraints. The first two columns of Table II compare constraints using C_ℓ^{TT} only to those using C_ℓ^{TT}, C_ℓ^{TE}, and C_ℓ^{EE}. Since all parameter shifts are substantially less than 1σ, we conclude that the isocurvature model considered here is insensitive to any residual $T \to E$ leakage. Henceforth we use Planck temperature and polarization data.

Comparing the vanilla parameters in Table II to those in Table 3 of Ref. [40], we see that parameter shifts are less than 0.6σ except for σ_8 and τ, which both increase by $\approx 1\sigma$ when isocurvature is included. However, these increase together along their mutual degeneracy direction. Since the CMB constrains the combination $\sigma_8 \exp(-\tau)$ more tightly than either of these parameters individually, we expect σ_8 and τ to change in such a way that $\Delta\sigma_8/\sigma_8 \approx \Delta\tau$, which is consistent with the shifts seen in Table II.

Since $Q_n = 0$ is allowed at the 1σ level for the KK and NB models, and slightly more than 1σ for the PWR model, we conclude that Planck data alone do not significantly prefer any of the isocurvature models in the table. While there is a slight preference for $n_I \approx 2.7$ and $\kappa_\star \approx -0.5$, the 95% allowed regions for both of these parameters include nearly the full ranges $1 \le n_I \le 3.94$ and $\ln(1/50) \le \kappa_\star \le \ln(10)$. Figure 2 shows marginalized two-dimensional constraints on the isocurvature parameters in the KK model. Note that for the smallest $\kappa_\star$ values, the isocurvature spectrum is flat over most of the observable range, meaning that n_I is poorly constrained.

TABLE II. Constraints on ΛCDM with isocurvature using Planck 2015 data (P) alone. The first column uses only the TT data in order to test for the effects of $T \to E$ leakage on parameter constraints. For each parameter, the mean value as well as 68% and 95% upper and lower bounds are shown. In some cases, both lower bounds on Q_n are equal due to the prior $Q_n \ge 0$, implying that our results only provide an upper bound.

	KK, P(TT-only)	KK, P	NB, P	PWR, P
n_s	$0.9684^{+0.0073\ +0.014}_{-0.0071\ -0.014}$	$0.9658^{+0.0056\ +0.011}_{-0.0051\ -0.01}$	$0.9656^{+0.0049\ +0.011}_{-0.0054\ -0.01}$	$0.9646^{+0.0049\ +0.009}_{-0.0053\ -0.0092}$
σ_8	$0.851^{+0.023\ +0.043}_{-0.022\ -0.045}$	$0.844^{+0.019\ +0.036}_{-0.016\ -0.038}$	$0.843^{+0.018\ +0.035}_{-0.017\ -0.036}$	$0.841^{+0.021\ +0.036}_{-0.015\ -0.042}$
h	$0.6799^{+0.011\ +0.022}_{-0.011\ -0.022}$	$0.6765^{+0.0075\ +0.014}_{-0.0071\ -0.014}$	$0.6761^{+0.0067\ +0.014}_{-0.007\ -0.014}$	$0.6762^{+0.0058\ +0.015}_{-0.007\ -0.013}$
$\omega_{\rm c}$	$0.1184^{+0.0022\ +0.0046}_{-0.0023\ -0.0046}$	$0.119^{+0.0015\ +0.0031}_{-0.0017\ -0.0031}$	$0.119^{+0.0015\ +0.0031}_{-0.0015\ -0.003}$	$0.119^{+0.0015\ +0.0029}_{-0.0013\ -0.0033}$
$\omega_{\rm b}$	$0.02236^{+0.00027\ +0.00053}_{-0.00025\ -0.00049}$	$0.02228^{+0.00016\ +0.00032}_{-0.00017\ -0.00033}$	$0.02227^{+0.00017\ +0.00032}_{-0.00017\ -0.00033}$	$0.02228^{+0.00018\ +0.00032}_{-0.00016\ -0.0003}$
τ	$0.108^{+0.034\ +0.06}_{-0.028\ -0.063}$	$0.0976^{+0.026\ +0.049}_{-0.023\ -0.051}$	$0.0968^{+0.025\ +0.049}_{-0.023\ -0.049}$	$0.0904^{+0.026\ +0.048}_{-0.021\ -0.049}$
Q_n	$1.2^{+0.3\ +2.4}_{-1.2\ -1.2}$	$1.0^{+0.3\ +1.4}_{-1.0\ -1.0}$	$1.1^{+0.3\ +1.5}_{-1.1\ -1.1}$	$0.010^{+0.003\ +0.012}_{-0.010\ -0.010}$
n_I	$2.75^{+1.19\ +1.19}_{-0.44\ -1.3}$	$2.74^{+1.2\ +1.2}_{-0.66\ -1.2}$	$2.63^{+0.78\ +1.3}_{-0.65\ -1.2}$	$2.43^{+0.6\ +1.2}_{-0.53\ -1}$
$\kappa_\star$	$-0.57^{+1.4\ +2.5}_{-1.1\ -2.9}$	$-0.51^{+1.2\ +2.6}_{-1\ -2.5}$	$-0.52^{+1.3\ +2.6}_{-1.1\ -2.5}$	

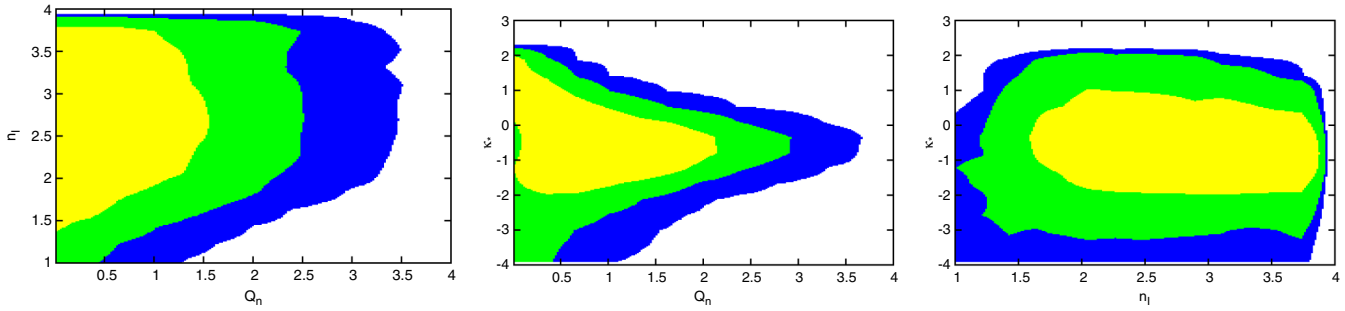

FIG. 2. Constraints on the KK model using Planck data. Light (yellow), medium (green), and dark (blue) shaded regions identify 68%, 95%, and 99.7% confidence contours, respectively.

C. Galaxy survey constraints

Next we combine the BOSS DR11 galaxy survey data with the Planck data. We begin by testing the robustness of our constraints with respect to the inclusion of additional parameters describing the scale-dependent bias. The first three columns of Table III constrain the KK model using Planck and BOSS data, marginalizing over the 5-parameter bias model of Ref. [36] for the first two columns and 3-parameter bias model for the other columns. Comparing the first and the third column, the constraints on h and ω_c shift by $\approx 0.3\sigma$, while all remaining parameters shift by less than 0.15σ, and the isocurvature parameters by $\lesssim 0.03\sigma$, suggesting that the 3-parameter bias model used henceforth (unless specified otherwise) provides robust constraints. Note that although allowing variations in the sum of the neutrino masses leads to an increase in the expectation value of κ_*, as can be seen in the second column, the shift is statistically insignificant since it is much smaller than a 1σ variation.

Comparing Planck + BOSS isocurvature constraints (e.g., the third column of Table III) to the Planck-only constraints of Table II, we see that $\kappa_\star$ increases by ≈ 0.3 with the addition of galaxy survey data, while $\ln(\sigma_8)$ and τ both drop by ≈ 0.03 in a way that leaves $\sigma_8 \exp(-\tau)$ nearly constant. As with the Planck-only analysis, we see that $Q_n = 0$ is allowed at 1σ in the KK and NB models, and at somewhat more than 1σ in the PWR model, indicating no significant preference for these isocurvature models. Once again, nearly the entire range of n_I and $\kappa_\star$ are within the 95% confidence regions. Comparing the two-dimensional constraints in Fig. 3 to those in Fig. 2, we see slight hints of a preference for higher $\kappa_\star$, n_I, and Q_n when galaxy survey data are included.

As another method of testing the significance of this preference, we compare the full set of chain points for each analysis to a negligible-isocurvature subset for which $Q_n < 0.1$ and $\kappa_\star < 0$. Although χ^2/degrees-of-freedom does not make sense as a goodness-of-fit test for

TABLE III. Constraints on ΛCDM with isocurvature using Planck 2015 (P) and BOSS DR11 (B) data. The first column analyzes the KK model using two extra scale-dependent bias parameters in order to test the robustness of our constraints, and the second column varies the sum of neutrino masses $\sum m_\nu = 93.14\omega_\nu$ eV as well as these extra bias parameters. For each parameter, the mean value as well as 68% and 95% upper and lower bounds are shown. In some cases, both lower bounds on Q_n are equal due to the prior $Q_n \geq 0$, implying that our results only provide an upper bound.

	KK + b_5, PB	KK + ω_ν + b_5, PB	KK, PB	NB, PB	PWR, PB
n_s	$0.9653^{+0.0041\ +0.0081}_{-0.0042\ -0.0086}$	$0.9668^{+0.0048\ +0.0095}_{-0.0047\ -0.01}$	$0.965^{+0.0042\ +0.0085}_{-0.0045\ -0.0084}$	$0.9651^{+0.0041\ +0.0086}_{-0.0043\ -0.0086}$	$0.9639^{+0.0043\ +0.0089}_{-0.0044\ -0.0086}$
σ_8	$0.821^{+0.018\ +0.034}_{-0.017\ -0.035}$	$0.809^{+0.021\ +0.036}_{-0.015\ -0.036}$	$0.818^{+0.018\ +0.034}_{-0.018\ -0.034}$	$0.819^{+0.018\ +0.033}_{-0.018\ -0.037}$	$0.814^{+0.016\ +0.032}_{-0.02\ -0.032}$
h	$0.6768^{+0.0052\ +0.0093}_{-0.0045\ -0.0098}$	$0.6717^{+0.0069\ +0.012}_{-0.0057\ -0.013}$	$0.6764^{+0.0048\ +0.0099}_{-0.005\ -0.0098}$	$0.6762^{+0.005\ +0.01}_{-0.005\ -0.01}$	$0.6767^{+0.0047\ +0.01}_{-0.0052\ -0.0095}$
ω_c	$0.1188^{+0.001\ +0.0021}_{-0.0011\ -0.002}$	$0.1183^{+0.0011\ +0.0029}_{-0.0014\ -0.0025}$	$0.1189^{+0.0011\ +0.0021}_{-0.0011\ -0.0022}$	$0.119^{+0.0011\ +0.0022}_{-0.0012\ -0.0022}$	$0.1189^{+0.0012\ +0.0021}_{-0.0011\ -0.0023}$
ω_b	$0.02226^{+0.00013\ +0.00028}_{-0.00014\ -0.00028}$	$0.0223^{+0.00015\ +0.0003}_{-0.00016\ -0.0003}$	$0.02227^{+0.00014\ +0.00029}_{-0.00014\ -0.00028}$	$0.02225^{+0.00013\ +0.00028}_{-0.00015\ -0.00028}$	$0.02226^{+0.00014\ +0.00029}_{-0.00015\ -0.00028}$
ω_ν		$0.0014^{+0.0005\ +0.0016}_{-0.0011\ -0.0014}$			
τ	$0.071^{+0.024\ +0.043}_{-0.02\ -0.045}$	$0.082^{+0.032\ +0.049}_{-0.027\ -0.058}$	$0.067^{+0.025\ +0.043}_{-0.022\ -0.051}$	$0.067^{+0.025\ +0.044}_{-0.024\ -0.047}$	$0.054^{+0.021\ +0.042}_{-0.03\ -0.044}$
Q_n	$1.0^{+0.3\ +1.3}_{-1.0\ -1.0}$	$1.1^{+0.3\ +1.5}_{-1.0\ -1.1}$	$0.96^{+0.32\ +1.3}_{-0.93\ -0.96}$	$1.1^{+0.3\ +1.4}_{-1.0\ -1.1}$	$0.012^{+0.005\ +0.012}_{-0.009\ -0.012}$
n_I	$2.72^{+1.2\ +1.2}_{-0.69\ -1.2}$	$2.78^{+1.1\ +1.2}_{-0.59\ -1.2}$	$2.76^{+1.1\ +1.2}_{-0.59\ -1.2}$	$2.65^{+0.75\ +1.2}_{-0.7\ -1.2}$	$2.65^{+0.69\ +0.92}_{-0.4\ -1.1}$
$\kappa_\star$	$-0.37^{+1.5\ +2.6}_{-0.98\ -2.7}$	$-0.21^{+1.3\ +2.5}_{-1.1\ -2.5}$	$-0.21^{+1.5\ +2.5}_{-1.1\ -2.4}$	$-0.31^{+1.5\ +2.6}_{-1.2\ -2.4}$	

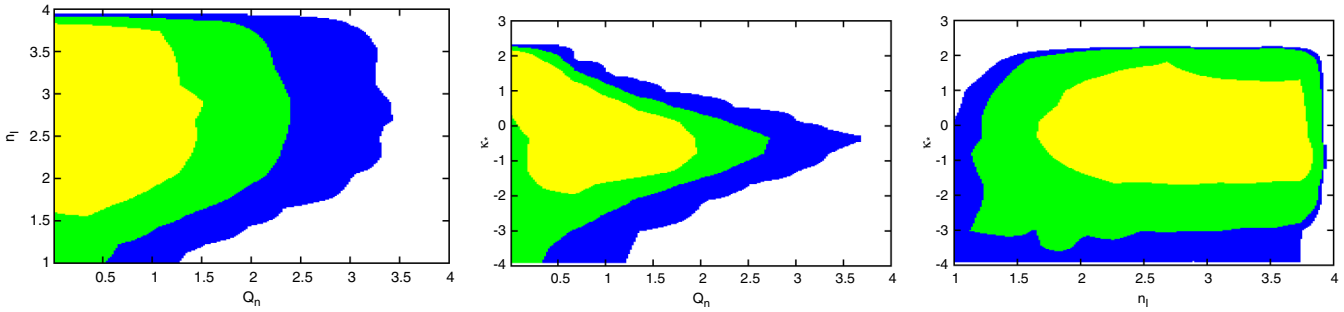

FIG. 3. Constraints on the KK model using Planck and BOSS DR11 data. Light (yellow), medium (green), and dark (blue) shaded regions identify 68%, 95%, and 99.7% confidence contours, respectively.

marginalized likelihoods such as the Planck likelihood, we can still ask whether varying 3 isocurvature parameters lowers the χ^2 by substantially more than 3. Allowing non-negligible isocurvature in the KK model reduces χ^2 by 2.4 in the Planck-only analysis and by 4.4 in the Planck + BOSS analysis. (A similar comparison to the vanilla Planck + BOSS analysis of Ref. [30] shows a χ^2 reduction of 4.8.) If we additionally allow all 5 bias parameters to vary in the Planck + BOSS analysis, the χ^2 reduction falls to 3.5. Thus there is not a strong preference for axionic blue isocurvature in the current data.

KK-type isocurvature models with different $\kappa_\star$ are qualitatively very different. In the small-$\kappa_\star$ limit, the KK model reduces to a flat isocurvature, with weak constraints on n_I coming only from cosmic-variance-limited measurements at horizon scales. Thus we consider a few specific lamppost models in which $\kappa_\star$ is fixed to larger values, in which current data can probe the blue-tilted region of the power spectrum. Table IV and Fig. 4 show the resulting constraints. We have chosen the maximum $\kappa_\star$ to be $\ln(0.5/\mathrm{Mpc}/k_0) = 2.3$, just beyond the largest wave numbers probed by Planck and BOSS data. In all three cases considered, with $\kappa_\star \geq 0$, we see a $> 1\sigma$ preference for $Q_n > 0$.

Finally, since we are specifically interested the bluest-tilted models, we consider lamppost models in which $n_I = 3.9$ is fixed (this value is 2σ allowed by the third column of Table III and lies at the maximum of the allowed MCMC sampling). Constraints on BLUE (variable-$\kappa_\star$) and HI-BLUE ($\kappa_\star = \ln(10)$) models are shown in the final two columns of Table IV. Intriguingly, the HI-BLUE model has a 2σ preference for $Q_n > 0$. We investigate this further in Table V, showing constraints with and without BOSS data. The corresponding one-dimensional probability density is shown in Fig. 5. Even though this is encouraging, this does not represent a statistically significant hint since there is no *a priori* reason to prefer the HI-BLUE spectrum for the fits.

Since $\kappa_\star = \ln(10)$ corresponds to $k_\star/a_0 = 0.5/\mathrm{Mpc} \approx 0.7h/\mathrm{Mpc}$, a few times larger than currently-accessible scales, this constraint can be interpreted as a 2σ preference for a highly blue-tilted isocurvature with a power-law spectrum on observable scales if there is some reason to expect $n_I = 3.9$ *a priori*. While a 2σ hint is hardly

TABLE IV. Constraints on lamppost models using Planck and BOSS data. LAMP-N is KK with $\kappa_\star = \ln(N)$, BLUE is KK with $n_I = 3.9$, and HI-BLUE is BLUE with $\kappa_\star = \ln(10)$. For each parameter, the mean value as well as 68% and 95% upper and lower bounds are shown. In some cases, both lower bounds on Q_n are equal due to the prior $Q_n \geq 0$, implying that our results only provide an upper bound.

	LAMP-1, PB	LAMP-2, PB	LAMP-10, PB	BLUE, PB	HI-BLUE, PB
n_s	$0.9653^{+0.0044\ +0.0086}_{-0.0044\ -0.0085}$	$0.9651^{+0.0041\ +0.0086}_{-0.0044\ -0.0083}$	$0.9637^{+0.0039\ +0.0084}_{-0.0045\ -0.0084}$	$0.9649^{+0.0041\ +0.0085}_{-0.0044\ -0.0085}$	$0.962^{+0.0045\ +0.0078}_{-0.0038\ -0.0082}$
σ_8	$0.819^{+0.019\ +0.033}_{-0.018\ -0.035}$	$0.817^{+0.017\ +0.034}_{-0.019\ -0.034}$	$0.814^{+0.015\ +0.033}_{-0.019\ -0.033}$	$0.819^{+0.019\ +0.034}_{-0.019\ -0.038}$	$0.812^{+0.014\ +0.032}_{-0.018\ -0.027}$
h	$0.6761^{+0.0047\ +0.0097}_{-0.0051\ -0.0096}$	$0.6766^{+0.0051\ +0.01}_{-0.0051\ -0.0099}$	$0.6765^{+0.0047\ +0.01}_{-0.0051\ -0.0096}$	$0.6762^{+0.0049\ +0.0099}_{-0.0048\ -0.0096}$	$0.6771^{+0.0047\ +0.0098}_{-0.0052\ -0.0095}$
ω_c	$0.119^{+0.0011\ +0.0022}_{-0.0011\ -0.0022}$	$0.1189^{+0.0011\ +0.0022}_{-0.0011\ -0.0022}$	$0.1189^{+0.0012\ +0.0021}_{-0.001\ -0.0022}$	$0.119^{+0.001\ +0.0021}_{-0.0011\ -0.0021}$	$0.1188^{+0.001\ +0.0022}_{-0.0012\ -0.0021}$
ω_b	$0.02226^{+0.00014\ +0.00028}_{-0.00014\ -0.00028}$	$0.02228^{+0.00014\ +0.00029}_{-0.00014\ -0.00028}$	$0.02228^{+0.00014\ +0.0003}_{-0.00015\ -0.00029}$	$0.02226^{+0.00015\ +0.0003}_{-0.00015\ -0.00029}$	$0.02227^{+0.00016\ +0.00028}_{-0.00013\ -0.00028}$
τ	$0.068^{+0.024\ +0.044}_{-0.023\ -0.044}$	$0.065^{+0.023\ +0.043}_{-0.024\ -0.046}$	$0.056^{+0.021\ +0.041}_{-0.028\ -0.046}$	$0.067^{+0.025\ +0.044}_{-0.024\ -0.049}$	$0.046^{+0.018\ +0.04}_{-0.032\ -0.036}$
Q_n	$1.4^{+0.7\ +1.4}_{-1.0\ -1.4}$	$0.93^{+0.42\ +0.85}_{-0.58\ -0.93}$	$0.19^{+0.062\ +0.2}_{-0.15\ -0.19}$	$1.1^{+0.3\ +1.3}_{-1.0\ -1.1}$	$0.062^{+0.026\ +0.049}_{-0.03\ -0.052}$
n_I	$2.75^{+0.8\ +1.2}_{-0.67\ -1.1}$	$2.77^{+0.85\ +1.2}_{-0.61\ -1.1}$	$2.75^{+0.77\ +1.2}_{-0.65\ -1.1}$		
$\kappa_\star$				$-0.45^{+1.2\ +2.2}_{-0.89\ -2.2}$	

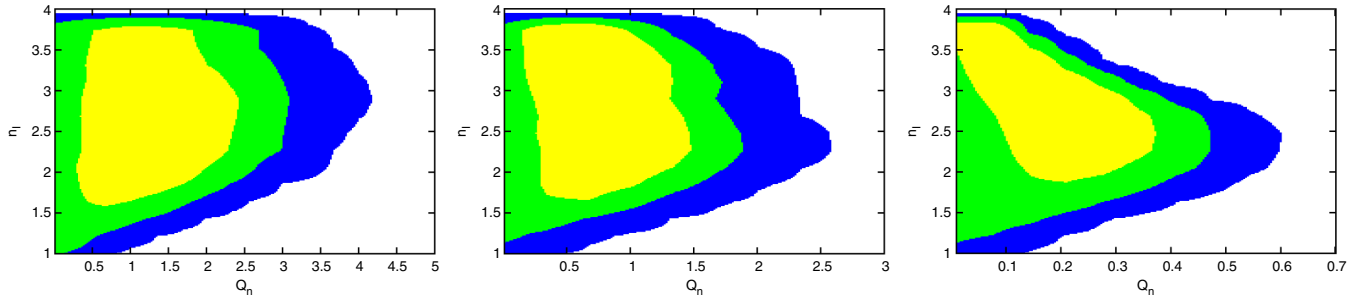

FIG. 4. Constraints on the LAMP-1 (left), LAMP-2 (middle), and LAMP-10 (right) models using Planck and BOSS DR11 data. Light (yellow), medium (green), and dark (blue) shaded regions identify 68%, 95%, and 99.7% confidence contours, respectively.

conclusive and there is no compelling reason to expect $n_I = 3.9$, if we interpret this really as a hint, there is some reason to be optimistic about its case being strengthened by data in the near future. Planned CMB and large-scale structure surveys promise more sensitivity over a larger range of scales. Surveys mapping the neutral hydrogen in the universe using the 21 cm line are expected to reach $k/a_0 \sim 10h/\mathrm{Mpc}$ in the coming decades. Such probes will shed light on physics at the highest energies through their sensitivity to ABI models.

Regardless of this fit result being interpreted as a hint, note that this class of models also "predicts" $k_\star$, the break point in the spectrum, to be in the observable range if one restricts the theoretical bias to having sub-Planckian scalar field values and more importantly the total number of e-folds of inflation not being smaller than around 50. More specifically, one can see from generalizing the model dependent Eq. (19) that

$$\frac{k_\star}{a_0} \sim \left(\frac{\varphi_{\mathrm{init}}}{0.3M_p}\right)^{\frac{2}{3}} e^{-(N_e-50)} \left(\frac{T_{\mathrm{rh}}/H}{10^{-1}}\right)^{1/3} \left(\frac{H/\varphi_{\mathrm{fin}}}{10^{-3}}\right)^{2/3} \times (10\ \mathrm{Mpc}^{-1}) \tag{7}$$

where M_p is the reduced Planck mass, H is the expansion rate during inflation, and φ is a model dependent order parameter that controls whether the isocurvature perturbation modes are massive or massless (when compared to H) at the time of mode horizon exit. In an axion model specific to Eq. (19), φ has the order of magnitude of the PQ symmetry-breaking field $|\Phi_+|$. The variable φ_{init} is the φ value at N_e e-folds before the end of inflation, and the variable φ_{fin} is the φ value at the time when the modes are first massless at horizon exit.

Another positive indication for future observability of this class of models can be seen as follows. According to column 4 of Table V, the 95% confidence level upper bound on Q_n is 0.11, which corresponds to $\mathcal{Q}_1 \approx 9 \times 10^{-8}$. This implies that the isocurvature power at $k/a_0 \gtrsim 0.5\ \mathrm{Mpc}^{-1}$ primordially can be 40 times larger than the adiabatic power (in contrast with the percent level power of a scale-invariant spectrum). Moreover, because the data set used here is already insensitive to the spectrum at this large $k/a_0 \gtrsim k_\star/a_0 \approx 0.5\ \mathrm{Mpc}^{-1}$, it is possible to dramatically further increase the isocurvature power relative to the adiabatic power by increasing $k_\star/a_0$.

TABLE V. Constraints on extremely blue-tilted lamppost models with $n_I = 3.9$. BLUE allows $\kappa_\star$ to vary while HI-BLUE fixes it at ln (10). Constraints are from Planck data alone (P) or Planck plus BOSS (PB). For each parameter, the mean value as well as 68% and 95% upper and lower bounds are shown. In some cases, both lower bounds on Q_n are equal due to the prior $Q_n \geq 0$, implying that our results only provide an upper bound.

	BLUE, P	HI-BLUE, P	BLUE, PB	HI-BLUE, PB
n_s	$0.9657^{+0.0051\ +0.01}_{-0.0052\ -0.01}$	$0.9628^{+0.0046\ +0.0099}_{-0.0048\ -0.01}$	$0.9649^{+0.0041\ +0.0085}_{-0.0044\ -0.0085}$	$0.962^{+0.0045\ +0.0078}_{-0.0038\ -0.0082}$
σ_8	$0.844^{+0.019\ +0.035}_{-0.017\ -0.037}$	$0.838^{+0.022\ +0.035}_{-0.02\ -0.042}$	$0.819^{+0.019\ +0.034}_{-0.019\ -0.038}$	$0.812^{+0.014\ +0.032}_{-0.018\ -0.027}$
h	$0.6764^{+0.0069\ +0.014}_{-0.007\ -0.014}$	$0.6767^{+0.0069\ +0.014}_{-0.0064\ -0.014}$	$0.6762^{+0.0049\ +0.0099}_{-0.0048\ -0.0096}$	$0.6771^{+0.0047\ +0.0098}_{-0.0052\ -0.0095}$
ω_c	$0.119^{+0.0015\ +0.0031}_{-0.0016\ -0.0031}$	$0.1189^{+0.0014\ +0.003}_{-0.0015\ -0.003}$	$0.119^{+0.001\ +0.0021}_{-0.0011\ -0.0021}$	$0.1188^{+0.001\ +0.0022}_{-0.0012\ -0.0021}$
ω_b	$0.02228^{+0.00017\ +0.00033}_{-0.00016\ -0.00033}$	$0.0223^{+0.00017\ +0.00032}_{-0.00016\ -0.00032}$	$0.02226^{+0.00015\ +0.0003}_{-0.00015\ -0.00029}$	$0.02227^{+0.00016\ +0.00028}_{-0.00013\ -0.00028}$
τ	$0.098^{+0.026\ +0.048}_{-0.023\ -0.051}$	$0.081^{+0.03\ +0.05}_{-0.026\ -0.057}$	$0.067^{+0.025\ +0.044}_{-0.024\ -0.049}$	$0.046^{+0.018\ +0.04}_{-0.032\ -0.036}$
Q_n	$1.1^{+0.3\ +1.5}_{-1.1\ -1.1}$	$0.047^{+0.024\ +0.044}_{-0.028\ -0.047}$	$1.1^{+0.31\ +1.3}_{-1\ -1.1}$	$0.062^{+0.026\ +0.049}_{-0.03\ -0.052}$
$\kappa_\star$	$-0.68^{+0.99\ +2.2}_{-0.79\ -2.2}$		$-0.45^{+1.2\ +2.2}_{-0.89\ -2.2}$	

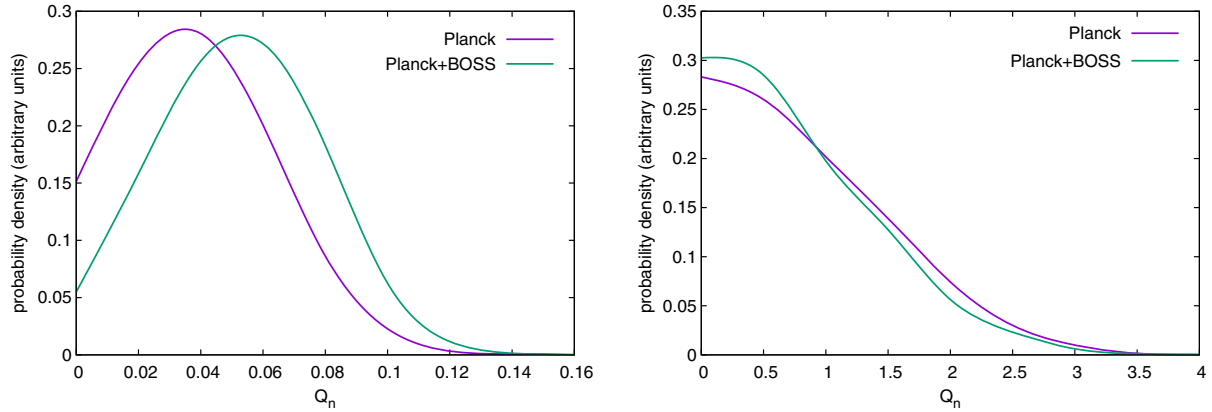

FIG. 5. Marginalized probability density of Q_n in (left) the HI-BLUE model, and (right) the full KK model, constrained using either Planck or Planck + BOSS data.

IV. A MODEL INTERPRETATION

In this section, we interpret the fit results of the last section in terms of the axion model of [17]. We will find that the fit is consistent with a very plausible supersymmetric QCD axion model. In particular, we will find that the result is consistent with a scenario in which all of the dark matter is composed of axions and the initial misalignment angle is of order unity.

The supersymmetric model [17] has its axion residing in a linear combination of PQ-charged beyond-the-Standard-Model fields Φ_+ and Φ_- where the subscripts refer to the PQ charges. As explained in [17] (and [18]), the relevant effective potential during inflation is

$$V \approx h_1^2|\Phi_+\Phi_- - F_a^2|^2 + c_+H^2|\Phi_+|^2 + c_-H^2|\Phi_-|^2 \quad (8)$$

where $\{h_1, c_\pm, F_a, H\}$ are numerical constants. The variable H has the interpretation of the expansion rate during inflation, and F_a is related to the usually quoted axion decay constant f_a through

$$f_a = \sqrt{2}(|\Phi_+(t_f)|^2 + |\Phi_-(t_f)|^2)^{1/2} \quad (9)$$

where

$$|\Phi_\pm(t_f)| = F_a\left(\frac{c_\mp}{c_\pm}\right)^{1/4}\sqrt{1 - \frac{\sqrt{c_+c_-}H^2}{h_1^2F_a^2}}. \quad (10)$$

Because of the insensitivity of the ABI spectrum with h_1-variation in the parameter region of interest, we can set $h_1 = 1$ as long as $h_1F_a \gg H$. The initial condition for $\Phi_\pm$ is parameterized by

$$\Phi_\pm(t_i) = |\Phi_\pm(t_i)|e^{\mp i\theta_+(t_i)} \quad (11)$$

where $\theta_+(t_i) \sim O(0.1)$ for "natural" scenarios.

The key initial condition is that $\{|\Phi_+(t_i)| \gg F_a, \Phi_+(t_i)\Phi_-(t_i) \approx F_a^2\}$ and Φ_+ rolls towards the minimum during inflation. With the parameterization

$$\Phi_\pm \equiv \frac{\varphi_\pm}{\sqrt{2}}\exp\left(i\frac{a_\pm}{\sqrt{2}\varphi_\pm}\right) \quad (12)$$

where $\varphi_\pm$ and $a_\pm$ are real, the axion is

$$a = \frac{\varphi_+}{\sqrt{\varphi_+^2 + \varphi_-^2}}a_+ - \frac{\varphi_-}{\sqrt{\varphi_+^2 + \varphi_-^2}}a_- \quad (13)$$

and this field will have a mass-squared that is approximately c_+H^2 during inflation if $|\Phi_+| \gg F_a$ while $\Phi_+\Phi_- = F_a^2$. The Goldstone theorem is evaded because the radial field Φ_+ is rolling and not at its minimum. This temporary massive behavior of the axion is responsible for the blueness of the ABI spectrum. The approximate constant behavior of the mass until Φ_+ reaches $\Phi_+(t_f)$ is natural within supersymmetric models since the leading SUSY breaking is controlled through gravity-mediated contribution H, the expansion rate, which is approximately constant during inflation.

As explained in [24], the parameter $\mathcal{Q}_1$ (related to the more practical fit parameter Q_n through Eq. (5) fixed through the fit constrains underlying model parameters through

$$\mathcal{Q}_1 = \left(\frac{H}{2\pi}\right)^2\frac{\tilde{A}(c_+)\sqrt{c_-/c_+}}{F_a^2\theta_+^2(t_i)(1 + c_-/c_+)}\omega_a^2 \quad (14)$$

where $\omega_a \equiv \Omega_a/\Omega_c$ is the dark matter fraction in axions and is approximately

$$\omega_a \approx W_a\theta_+^2(t_i)\left(\frac{\sqrt{2}F_a\sqrt{\frac{c_-+c_+}{\sqrt{c_-c_+}}}}{10^{12}\ \mathrm{GeV}}\right)^{n_{PT}}. \quad (15)$$

Here

$$W_a \approx 1.5 \qquad n_{PT} \approx 1.19 \tag{16}$$

are QCD phase transition physics related parameters [42], and we have assumed that $c_\pm > 0$. The ω_a parametric dependence assumes that the axion relic density is dominated by the coherent oscillations after the chiral phase transition. It also assumes that the coherent oscillations begin when $T \gtrsim 0.1$ GeV such that the axion mass has the usual nontrivial temperature dependence of $m_a \propto (\Lambda_{\rm QCD}/T)^{3.34}$ (see Eq. (9) of [42]). In terms of F_a, we are assuming $F_a \lesssim 10^{17}$ GeV. For larger F_a, the relic abundance formula needs modifications, but for this section, this will not be of interest to us because this parameter region is not phenomenologically viable. Although one can compute $\tilde{A}$ in terms of the interpolating function of [24], its range is

$$\tilde{A}(c_+) \approx 0.92 \pm 0.03 \tag{17}$$

which means one can obtain a good approximation without computing this accurately.

Combining Eqs. (5) and (14), we can write all the fit parameters on the right hand side of the equation

$$\frac{[H\theta_+(t_i)]^2 F_a^{2n_{PT}-2}}{(10^{12}\ {\rm GeV})^{2n_{PT}}} = \frac{(2\pi)^2(1+c_-/c_+(n_I))^{1-n_{PT}}10^{-10}(1+e^{n_I\kappa_\star})Q_n}{2^{n_{PT}}\tilde{A}(c_+)(\sqrt{c_-/c_+(n_I)})^{1-n_{PT}}W_a^2} \tag{18}$$

where Eqs. (4), (16), and (17) and the parametric choice $\{c_- = 0.9, n_I > 1.68\}$ can be used to complete the specification of the right hand side.[2] For every right hand side of Eq. (18) specified by the fit, this equation allows us to have an area of solutions in $(H, \theta_+(t_i), F_a)$ space. For every point in the solution space, there is a $\kappa_\star$ related constraint in the inflationary model/initial condition parameter $(T_{rh}, N_e, |\Phi_+(t_i)|)$ space through the following equation which relates observable length scales to these inflationary parameters:

$$\left(\frac{|\Phi_+(t_i)|}{F_a}\right)^{\frac{1}{\gamma}} e^{-(N_e-54)}\left(\frac{T_{\rm rh}}{10^7\ {\rm GeV}}\right)^{1/3}\left(\frac{H}{7\times 10^8\ {\rm GeV}}\right)^{1/3} = \frac{e^{\kappa_\star}}{2\times 10^{-4}}\left(\frac{c_+(n_I)}{c_-}\right)^{-\frac{1}{4\gamma(n_I)}} \tag{19}$$

[2]See the discussion below Eq. (1) and the discussion in [24] for more information about the c_- parametric choice.

where

$$\gamma(n_I) = \frac{3}{2}\left(1-\sqrt{1-\frac{4}{9}c_+(n_I)}\right). \tag{20}$$

Here, T_{rh} is the reheating temperature (temperature at which the universe becomes radiation dominated after inflation), N_e is the number of e-folds between an initial time t_i and the end of inflation, and $g_{*S}(t_0)$ is the effective number of entropy d.o.f. today. Because of the exponential on the left hand side of Eq. (19), the exponential variations in $\kappa_\star$ can easily be accommodated in variations in N_e. As we will see more explicitly shortly, this means that the break in the spectrum can be placed almost anywhere in the observable length scales as long as the number of e-folds of inflation is not strongly constrained. For an example of assumptions that can lead to constraints, see the discussion around Eq. (7).

Recall that the mean and 68% CL range for the spectral index are

$$n_I = 2.8^{+1.1}_{-0.6}(1\sigma) \tag{21}$$

taken from the third column of Table III. Given that the right hand side of Eqs. (18) and (19) only contain fit parameters, we plot in Fig. 6 the $(X_{\rm phen}, Y_{\rm phen})$ distribution generated by MCMC for bins of n_I surrounding the mean spectral index of Eq. (21) where

$$X_{\rm phen} \equiv \frac{(2\pi)^2(1+c_-/c_+(n_I))^{1-n_{PT}}10^{-10}(1+e^{n_I\kappa_\star})Q_n}{2^{n_{PT}}\tilde{A}(c_+)(\sqrt{c_-/c_+(n_I)})^{1-n_{PT}}W_a^2} \tag{22}$$

$$Y_{\rm phen} \equiv \frac{e^{\kappa_\star}}{2\times 10^{-4}}\left(\frac{c_+(n_I)}{c_-}\right)^{-\frac{1}{4\gamma(n_I)}} \tag{23}$$

and the Q_n dependence shows up only in $X_{\rm phen}$. As explained in the figure captions, the results suggest that much of the constraint for the $n_I \gtrsim 3$ models with the current data is coming from the bump region and above in k space since that part of the data is not as sensitive to the spectral index for $\kappa_\star < 0$. The insensitivity of the $k \gtrsim k_0 \exp(\kappa_\star)$ part of the spectrum with the spectral index n_I is illustrated in Fig. 7. On the other hand, the likelihood for the $n_I < 2.8$ region is more sensitive to the data with k smaller than the break (and hence the likelihood is more sensitive to the spectral index) since the isocurvature amplitude there is not as suppressed in the case of the smaller spectral index. This also explains the asymmetry in the error bars in Eq. (21). Note that because CMB observables are not as sensitive to large k isocurvature primordial spectrum compared to the large k adiabatic primordial spectrum, the $k < k_\star$ part of the spectrum in

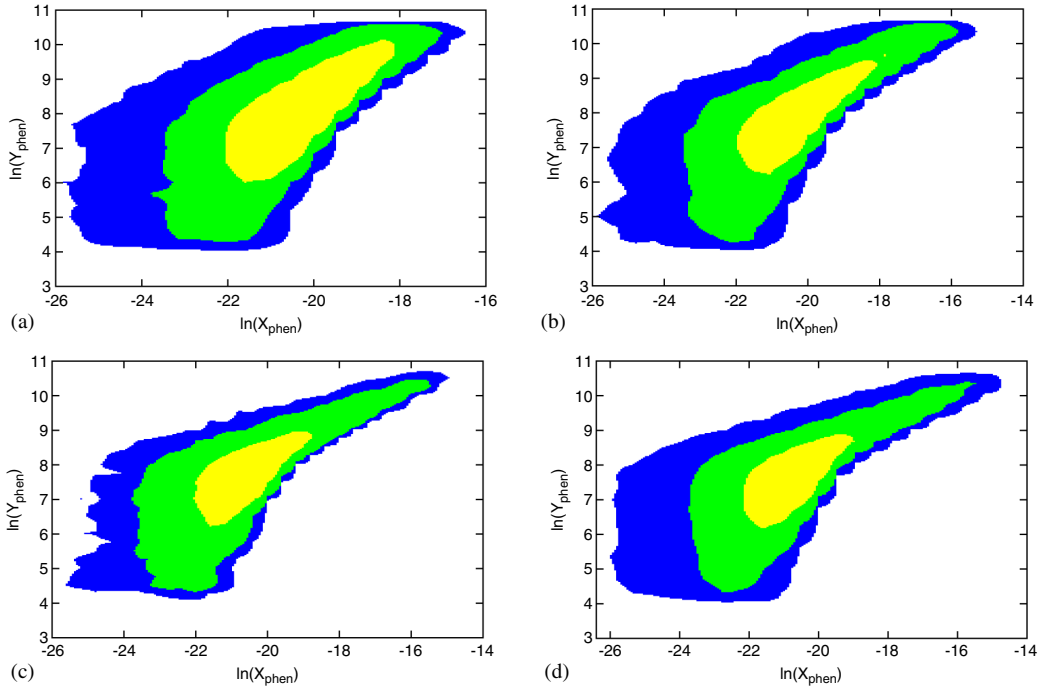

FIG. 6. Distribution of $(X_{\rm phen}, Y_{\rm phen})$ (with CMB only KK fit) is plotted for (a) $n_I \in [1.9, 2.3]$, (b) $n_I \in [2.6, 2.9]$, and (c) $n_I \in [3.54, 3.94]$ (d) BLUE model with $n_I = 3.9$. Each successive contoured regions corresponds to 1,2,3-σ regions. Since the distributions (c) and (d) are similar, the constraint is not very sensitive to the isocurvature spectral index n_I "far" above the central spectral index of Eq. (21). This suggests that much of the constraint for the "large" n_I models with the current data is coming from the bump region and above in k space since that part of the data is not as sensitive to the spectral index for $\kappa_\star < 0$.

Fig. 7 is more significant for CMB fits than it naively appears for shallow n_I.

Inspired by the fit results of Fig. 6, Eq. (21), and Sec. III, we choose two representative parameter sets to investigate

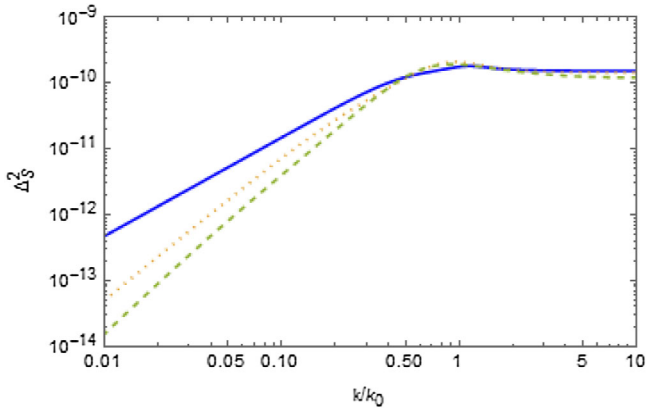

FIG. 7. $\Delta_S^2(k, k_\star, n_I, \mathcal{Q}_1)$ is plotted for $n_I = 2.5$ (solid), $n_I = 3.2$ (dotted), and $n_I = 3.9$ (dashed) with $k_\star = 0.81 k_0$ and $Q_n = 0.96$. The bump region and above are not very sensitive to the spectral index for a fixed Q_n. The plateau amplitude (corresponding to the mean n_I) is approximately 10% of the adiabatic power, which represents an order of magnitude enhancement compared to the current bounds on the flat spectral index case.

whether interpreting these parameters in terms of the axion model of [17] leads to a reasonable physical picture. One set we choose is the expectation values $S_1 \equiv \{n_I = 2.8, X_{\rm phen} = \exp(-20.6), Y_{\rm phen} = \exp(8.1)\}$ (corresponding to $\{Q_n = 0.96, \kappa_\star = -0.21, \mathcal{Q}_1 = 1.5 \times 10^{-10}\}$) and a second set $S_2 \equiv \{n_I = 2.8, X_{\rm phen} = \exp(-19.8), Y_{\rm phen} = \exp(7.7)\}$ (corresponding to $\{Q_n = 2.8, \kappa_\star = -0.6, \mathcal{Q}_1 = 3.3 \times 10^{-10}\}$) which gives a larger Q_n that is still 1σ consistent with the central value in the binned distribution of Fig. 6(b). The $\{\theta_+(t_i), H, F_a\}$ parameter regions consistent with S_1 and S_2 are shown in Fig. 8. The most important phenomenological self-consistency constraint in Fig. 8 is that the axion dark matter does not exceed the totality of cold dark matter abundance:

$$\omega_a \leq 1. \tag{24}$$

This determines the upper ends of each of the allowed (H, F_a) curves. The most important theoretical constraint comes from the validity of the linear computation,

$$\frac{\sqrt{\Delta_S^2}}{\omega_a} < 1, \tag{25}$$

which is a restatement of the assumed smallness of axion energy overdensity $\delta\rho_a/\rho_a < 1$. Since the spectral peak is

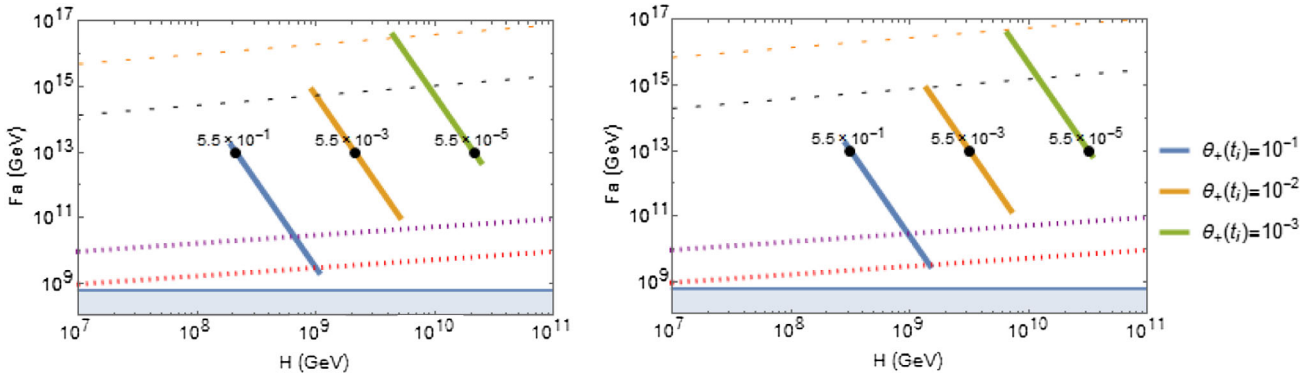

FIG. 8. Shown are axionic parameter regions consistent with the parameters S_1 preferred by current data (left) and a larger Q_n parameter set S_2 (right). Hence, the effect of increasing Q_n and adjusting $\kappa_\star$ to maintain a good fit to the data shifts the underlying model parameters $\{H, F_a\}$ to the right. The upper ends on all the thick lines come from the saturation of the dark matter bound: $\omega_a \leq 1$. The bottom ends on all the thick lines come from the bound of perturbativity: $\delta\rho_a/\rho_a < 1$. The dashed curves represent $|\Phi_+(t_i)| < 0.3M_p$ with two different numbers of inflationary e-folds. The upper one assumes that the number of e-folds N_e of inflation is at least 50, while the second curve assumes that the number of e-folds of inflation is at least 54. The dotted curves towards the bottom of the figure represent boundaries below which the total dark matter abidance may also contain cosmic strings because the maximum temperature reached during the reheating period is larger than F_a. The upper dotted curve is for $T_{rh} = 10^8$ GeV while the lower dotted curve is for $T_{rh} = 10^6$ GeV. The bottom blue region is excluded by the supernova 1987A burst duration (e.g., [43]), and some literature exclude F_a values that are an order of magnitude higher [10]. The numbers by the isolated dots indicate ω_a at that point in the parameter space.

less than about twice the plateau, we can impose a simpler bound,

$$\frac{\mathcal{Q}_1}{\omega_a} < \frac{1}{2}, \tag{26}$$

which will set a lower bound on F_a. This determines the lower ends of each of the allowed (H, F_a) curves.

The dashed curves in Fig. 8 represent $|\Phi_+(t_i)| < 0.3M_p$ with two different numbers of inflationary e-folds. If $|\Phi_+(t_i)|$ is above this value, we would generically be wary of the breakdown of the effective field theory description that neglects gravity suppressed nonrenormalizable operators. Note that N_e in Eq. (19) represents the number of e-folds between time t_i and the end of inflation. Hence, we see from the figure that the initial nonequilibrium value of $|\Phi_+(t_i)|$ need not be very large to satisfy the best fit value of $\kappa_\star$. The dotted curves towards the bottom of the plot represent the boundary below which we would have to take into account the cosmic string decay contribution to the axionic dark matter abundance due to the fact that PQ symmetry might be restored if

$$F_a \lesssim T_{\max} = (0.77)\left(\frac{9}{5\pi^3 g_*}\right)^{1/8}\sqrt{T_{rh}}(HM_p\sqrt{8\pi})^{1/4}, \tag{27}$$

where $T_{\max}$ is taken from [44] and we have assumed in Fig. 8 that the number of d.o.f. g_* contributing to the energy density is 200 at the completion of reheating. If the axionic string network reaches the scaling regime, then the decay of the strings will contribute an axion abundance of [42]

$$\Omega_{a,\mathrm{str}} \approx 2.0\xi\left(\frac{F_a}{10^{12}\ \mathrm{GeV}}\right)^{1.19}\left(\frac{\Lambda_{\mathrm{QCD}}}{400\ \mathrm{MeV}}\right), \tag{28}$$

which would be relevant in the parameter regime below the dotted curve in Fig. 8. Since there is a large parameter region in which axions constitute all of the dark matter, we will not dwell on this parametric corner where the string contribution becomes important.

Some other constraints that we have considered but are not important in the best fit parameter region are the following. Making sure that the initial $\theta_+(t_i)$ tuning is above the quantum noise and noting the approximation made in Eq. (29) of [24], we impose

$$\frac{H}{2\pi|\Phi_+(t_i)|} \ll \theta_+(t_i) \ll 1. \tag{29}$$

If we require that the classical value of the conserved quantity be always greater than the quantum fluctuations (not just at the initial time), we end up with a stronger constraint:

$$\frac{H}{4\pi F_a\sqrt{c_- + c_+}} \ll \theta_+(t_i) \ll 1. \tag{30}$$

These constraints are not as strong as the ones playing a role in Fig. 8.

It is important to note that the axionic d.o.f. naturally carries both adiabatic and isocurvature inhomogeneity

condition information because of the gravitational coupling between the inflaton and the axion, as discussed in [18]. In spatially flat gauge, this imprinting of the adiabatic inhomogeneities shows up as a secular time integral effect. Hence, even though the axion is a spectator field with its own independent quantum fluctuations, it naturally acquires mixed boundary conditions.

V. CONCLUSIONS

In this work, we have fit the ABI spectrum to Planck and BOSS DR11 data. Unlike the usual isocurvature spectrum that is fit to data in the literature, this spectrum has a strong blue tilt up to $k_\star$, has a little bump, and is flat beyond that. We use the economical three-parameter fitting function of [24] in the context of six-parameter vanilla Λ-CDM and find the best-fit isocurvature parameter set of about $\{k_\star/a_0 = 4.1^{+14}_{-2.7} \times 10^{-2}\ \mathrm{Mpc}^{-1}, n_I = 2.76^{+1.1}_{-0.59}, Q_n = 0.96^{+0.32}_{-0.93}\}$ (1σ error bars) which indicates a decent fit with the ABI spectrum making up about 10% of the power on short scales. Unfortunately, it is clear that there is no statistical significance to this nonzero isocurvature amplitude. Note that 10% of the primordial power on short scales is much larger than what one would expect from a scale-invariant isocurvature spectrum. The rest of the Λ-CDM parameters can be found in Table III. If we fix the spectral index and the break point to be large ($n_I = 3.9$, $k_\star/a_0 = 0.7h/\mathrm{Mpc}$), we find a 2σ preference for a nonzero ABI spectrum as indicated by Fig. 5. It is interesting to note that the 2σ acceptable fit of this HI-BLUE model allows the primordial isocurvature power to be 40 times the adiabatic primordial power at $k \gtrsim k_\star$ scales.

Furthermore, in the context of the axion model of [17], the parameter region preferred by current data corresponds to all of the dark matter being made up of QCD axions with the axion decay constant of order 10^{13} GeV and an expansion rate of order 10^8 GeV during inflation. This interpretation would imply no detection of inflaton generated gravity waves (tensor perturbations) in the near future (e.g., in experiments such as CMB-S4 [45]). However, the axion masses would be within the range of detectability through microwave cavity type of experiments [46]. Although all of these results are encouraging, the fit results are statistically inconclusive.

On the other hand, there is additional reason to have some optimism that the results might be hinting at a signal. As investigated by [29], a Λ-CDM fit to small l ($l \in [2, 1000)$) and the large l ($l \geq 1000$) Planck data gives about a 2σ discrepant value of $\Omega_c h^2$. In particular, the low-ℓ data prefers $\Omega_c h^2 \approx 0.115$ while the high-ℓ data prefers $\Omega_c h^2 \approx 0.125$. Although [29] disfavors this discrepancy as a hint for new physics because of the Planck data's tension with the South Pole Telescope data, the interpretation of this discrepancy is currently unresolved, and what we may be detecting in the ABI fit presented in this paper is this mismatch between the low-ℓ and high-ℓ data. For example, Ref. [29] considered the possibility of increasing a CMB lensing phenomenological parameter A_L (possibly motivated by modified gravity) to resolve the anomaly. The paper [47] shows that the A_L can be set to its general relativity value of $A_L = 1$ using compensated isocurvature perturbations. One can obtain a sense of how the ABI spectrum mimics the large $\Omega_c h^2$ effect in the large ℓ region through Fig. 9, which significantly exaggerates both $\Omega_c h^2$ and Q_n to make the effect more apparent.

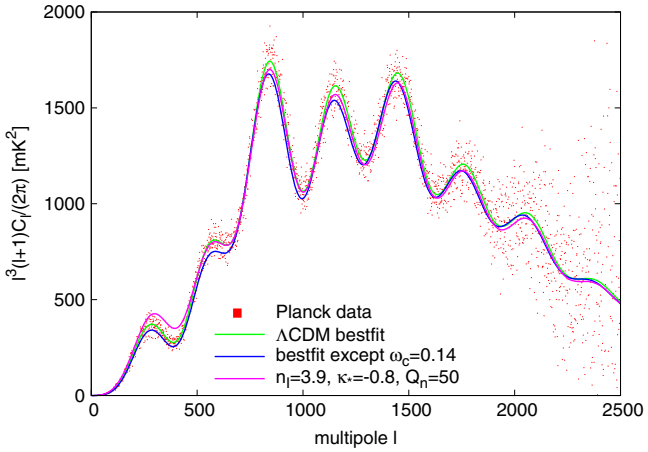

FIG. 9. Qualitative picture showing how an exaggeratedly large $\omega_c \equiv \Omega_c h^2$ Λ-CDM C_l prediction in the high-ℓ region is mimicked by the prediction with the addition of an exaggeratedly large ABI contribution.

Although future data may shed light on the systematics between the low ℓ and the high ℓ, the current state of the data seems unclear. For example, the SPTpol polarization data of [48] for $l < 1000$ are consistent with high $\Omega_c h^2$, while the data for $l > 1000$ prefer a large $\Omega_c h^2$. The ACTPol data of [49] have error bars that are consistent with both high and low $\Omega_c h^2$. Although the most probable interpretation of the low-ℓ vs high-ℓ anomaly can be argued to be the existence of not yet well understood systematics, if it is a signal of new physics, we can look forward to future data increasing the statistical significance of the hint. Indeed, planned CMB and large-scale structure surveys will improve data sensitivity over a larger range of scales. Since experiments measuring the 21 cm line are expected to reach scale sensitivities of $k/a_0 \sim 10h/\mathrm{Mpc}$ in the coming decades [50], such probes may shed light on physics at the highest energies by confirming or excluding hints of ABI perturbations.

ACKNOWLEDGMENTS

This work was supported in part by the Department of Energy through Grant No. DE-SC0017647. This research was performed using the computer resources and assistance of the UW-Madison Center For High Throughput

Computing (CHTC) in the Department of Computer Sciences. The CHTC is supported by UW-Madison, the Advanced Computing Initiative, the Wisconsin Alumni Research Foundation, the Wisconsin Institutes for Discovery, and the National Science Foundation, and is an active member of the Open Science Grid, which is supported by the National Science Foundation and the U.S. Department of Energy's Office of Science.

[1] R. Peccei and H. R. Quinn, CP Conservation in the Presence of Instantons, Phys. Rev. Lett. **38**, 1440 (1977).
[2] S. Weinberg, A New Light Boson?, Phys. Rev. Lett. **40**, 223 (1978).
[3] F. Wilczek, Problem of Strong p and t Invariance in the Presence of Instantons, Phys. Rev. Lett. **40**, 279 (1978).
[4] J. E. Kim, Weak Interaction Singlet and Strong *CP* Invariance, Phys. Rev. Lett. **43**, 103 (1979).
[5] M. A. Shifman, A. I. Vainshtein, and V. I. Zakharov, Can confinement ensure natural *CP* invariance of strong interactions?, Nucl. Phys. **B166**, 493 (1980).
[6] A. R. Zhitnitsky, On possible suppression of the axion hadron interactions. (In Russian), Sov. J. Nucl. Phys. **31**, 260 (1980).
[7] M. Dine, W. Fischler, and M. Srednicki, A simple solution to the strong *CP* problem with a harmless axion, Phys. Lett. B **104**, 199 (1981).
[8] J. E. Kim and G. Carosi, Axions and the strong *CP* problem, Rev. Mod. Phys. **82**, 557 (2010).
[9] P. Svrcek and E. Witten, Axions in string theory, J. High Energy Phys. 06 (2006) 051.
[10] M. P. Hertzberg, M. Tegmark, and F. Wilczek, Axion cosmology and the energy scale of inflation, Phys. Rev. D **78**, 083507 (2008).
[11] K. A. Malik and D. Wands, Cosmological perturbations, Phys. Rep. **475**, 1 (2009).
[12] M. Beltran, J. Garcia-Bellido, and J. Lesgourgues, Isocurvature bounds on axions revisited, Phys. Rev. D **75**, 103507 (2007).
[13] M. Bucher, J. Dunkley, P. Ferreira, K. Moodley, and C. Skordis, The Initial Conditions of the Universe: How Much Isocurvature Is Allowed?, Phys. Rev. Lett. **93**, 081301 (2004).
[14] P. Fox, A. Pierce, and S. D. Thomas, Probing a QCD string axion with precision cosmological measurements, arXiv: hep-th/0409059.
[15] G. Efstathiou and J. R. Bond, Isocurvature cold dark matter fluctuations, Mon. Not. R. Astron. Soc. **218**, 103 (1986).
[16] D. Seckel and M. S. Turner, Isothermal density perturbations in an axion dominated inflationary universe, Phys. Rev. D **32**, 3178 (1985).
[17] S. Kasuya and M. Kawasaki, Axion isocurvature fluctuations with extremely blue spectrum, Phys. Rev. D **80**, 023516 (2009).
[18] D. J. H. Chung and H. Yoo, Elementary theorems regarding blue isocurvature perturbations, Phys. Rev. D **91**, 083530 (2015).
[19] M. Dine, W. Fischler, and D. Nemeschansky, Solution of the entropy crisis of supersymmetric theories, Phys. Lett. B **136**, 169 (1984).
[20] O. Bertolami and G. G. Ross, Inflation as a cure for the cosmological problems of superstring models with intermediate scale breaking, Phys. Lett. B **183**, 163 (1987).
[21] E. J. Copeland, A. R. Liddle, D. H. Lyth, E. D. Stewart, and D. Wands, False vacuum inflation with Einstein gravity, Phys. Rev. D **49**, 6410 (1994).
[22] M. Dine, L. Randall, and S. D. Thomas, Supersymmetry Breaking in the Early Universe, Phys. Rev. Lett. **75**, 398 (1995).
[23] D. J. H. Chung, Large blue isocurvature spectral index signals time-dependent mass, Phys. Rev. D **94**, 043524 (2016).
[24] D. J. Chung and A. Upadhye, Bump in the blue axion isocurvature spectrum, Phys. Rev. D **95**, 023503 (2017).
[25] R. Adam *et al.*, X. Diffuse component separation: Foreground maps, Astron. Astrophys. **594**, A10 (2016).
[26] N. Aghanim *et al.*, XI. CMB power spectra, likelihoods, and robustness of parameters, Astron. Astrophys. **594**, A11 (2016).
[27] F. Beutler *et al.*, The clustering of galaxies in the SDSS-III Baryon Oscillation Spectroscopic Survey: Testing gravity with redshift space distortions using the power spectrum multipoles, Mon. Not. R. Astron. Soc. **443**, 1065 (2014).
[28] F. Beutler *et al.*, The clustering of galaxies in the SDSS-III Baryon Oscillation Spectroscopic Survey: Signs of neutrino mass in current cosmological data sets, Mon. Not. R. Astron. Soc. **444**, 3501 (2014).
[29] G. E. Addison, Y. Huang, D. J. Watts, C. L. Bennett, M. Halpern, G. Hinshaw, and J. L. Weiland, Quantifying discordance in the 2015 Planck CMB spectrum, Astrophys. J. **818**, 132 (2016).
[30] A. Upadhye, Neutrino mass and dark energy constraints from redshift-space distortions, arXiv:1707.09354.
[31] A. Lewis, A. Challinor, and A. Lasenby, Efficient computation of cosmic microwave background anisotropies in closed Friedmann-Robertson-Walker models, Astrophys. J. **538**, 473 (2000).
[32] H. K. Eriksen, J. B. Jewell, C. Dickinson, A. J. Banday, K. M. Gorski, and C. R. Lawrence, Joint Bayesian component separation and CMB power spectrum estimation, Astrophys. J. **676**, 10 (2008).
[33] A. Upadhye, J. Kwan, A. Pope, K. Heitmann, S. Habib, H. Finkel, and N. Frontiere, Redshift-space distortions in massive neutrino and evolving dark energy cosmologies, Phys. Rev. D **93**, 063515 (2016).
[34] M. Pietroni, Flowing with time: A new approach to nonlinear cosmological perturbations, J. Cosmol. Astropart. Phys. 10 (2008) 036.

[35] A. Upadhye, R. Biswas, A. Pope, K. Heitmann, S. Habib, H. Finkel, and N. Frontiere, Large-scale structure formation with massive neutrinos and dynamical dark energy, Phys. Rev. D **89**, 103515 (2014).
[36] P. McDonald and A. Roy, Clustering of dark matter tracers: Generalizing bias for the coming era of precision LSS, J. Cosmol. Astropart. Phys. 08 (**2009**) 020.
[37] S. Saito, T. Baldauf, Z. Vlah, U. Seljak, T. Okumura, and P. McDonald, Understanding higher-order nonlocal halo bias at large scales by combining the power spectrum with the bispectrum, Phys. Rev. D **90**, 123522 (2014).
[38] A. Gelman and D. B. Rubin, Inference from iterative simulation using multiple sequences, Stat. Sci. **7**, 457 (1992).
[39] S. P. Brooks and A. Gelman, General methods for monitoring convergence of iterative simulations, J. Comput. Graph. Stat. **7**, 434 (1997).
[40] P. A. R. Ade *et al.*, XIII. Cosmological parameters, Astron. Astrophys. **594**, A13 (2016).
[41] P. A. R. Ade *et al.*, XX. Constraints on inflation, Astron. Astrophys. **594**, A20 (2016).
[42] M. Kawasaki and K. Nakayama, Axions: Theory and cosmological role, Annu. Rev. Nucl. Part. Sci. **63**, 69 (2013).
[43] G. G. Raffelt, Astrophysical axion bounds, Lect. Notes Phys. **741**, 51 (2008).
[44] D. J. H. Chung, E. W. Kolb, and A. Riotto, Production of massive particles during reheating, Phys. Rev. D **60**, 063504 (1999).
[45] K. N. Abazajian *et al.* (CMB-S4 Collaboration), CMB-S4 science book, First Edition, arXiv:1610.02743.
[46] M. Battaglieri *et al.*, US cosmic visions: New ideas in dark matter 2017: Community report, arXiv:1707.04591.
[47] J. Valiviita, Power-spectra-based Planck constraints on compensated isocurvature, and forecasts for LiteBIRD and CORE space missions, J. Cosmol. Astropart. Phys. 04 (2017) 014.
[48] J. W. Henning *et al.* (SPT Collaboration), Measurements of the temperature and E-Mode polarization of the CMB from 500 square degrees of SPTpol data, Astrophys. J. **852**, 97 (2018).
[49] T. Louis *et al.* (ACTPol Collaboration), The Atacama Cosmology Telescope: Two-Season ACTPol spectra and parameters, J. Cosmol. Astropart. Phys. 06 (2017) 031.
[50] F. Villaescusa-Navarro, M. Viel, D. Alonso, K. K. Datta, P. Bull, and M. G. Santos, Cross-correlating 21 cm intensity maps with Lyman Break Galaxies in the post-reionization era, J. Cosmol. Astropart. Phys. 03 (2015) 034.